Computational Mechanics
https://doi.org/10.1007/s00466-022-02215-5

ORIGINAL PAPER

Thermal modeling and uncertainty quantification of tool for automated garment assembly

Nicolas Castrillon[1] · **Avery Rock**[1] · **Tarek I. Zohdi**[1]

Received: 5 April 2022 / Accepted: 12 July 2022

Abstract
In this work, a thermal Finite Element model is developed to simulate the performance of a blade-like tool for robotic work cells performing automated garment production using a novel thermoplastic stiffening layer. Uncertainty quantification and sensitivity analysis are applied to determine the most important design properties and optimize key performance metrics for swift and reliable garment assembly. Attention is focused on the geometric and thermal design properties that minimize sensitivity to environmental conditions while maximizing expected productivity. An example design is shown for illustrative purposes. This work may inform future design innovation for similar heating tools and reduce the need for physical experiments and long calibration times on the factory floor.

Keywords Uncertainty quantification · Finite element method · Thermal modeling · Automation · Garments

1 Introduction

1.1 Current state of the garments industry

The garment industry is a collection of supply chains, primarily comprised of fiber production, yarn and fabric production, and finally the assembly of consumer products.

While recent technological advances have enabled robots to manufacture high-value goods like car parts and electronics, the garment industry is still largely reliant on manual labor. Some assembly steps, such as attaching buttons and zippers, have been automated; these tasks are performed by single-purpose machines which are inherently more costly and more difficult to change between tasks compared to human workers. Little significant automation currently exists for the labor-intensive cutting and sewing steps required for garment assembly. With cheap labor readily available and international supply chains historically dependable, there has been little incentive to innovate [1,2]. However, there have been several recent initiatives put forth by non-governmental organizations, researchers, and other stakeholder organizations to calculate and determine local living wages for garment workers [3], generating pressures on clothing brands and factories to identify other cost-effective fabrication processes. For this reason and in the spirit of the Industrial Revolution 4.0, the development of automation technologies for cut-and-sew operations is a promising avenue for modernizing garment assembly supply chains.

1.2 Challenges with automation

On the technical side, handling limp textiles is more challenging for robots than handling rigid objects. Unlike a rigid body, a piece of fabric may be folded, wrinkled, or otherwise distorted, presenting challenges for both the mechanics of grasping and for computer vision algorithms. This makes manipulating textiles a challenge for robotic systems [4].

One method to address this challenge is to stiffen textiles during assembly and reverse the process once finished [5]. A novel process may be used to treat textiles with a thermoplastic laminating layer. The laminating material can be removed with hot water to produce a conventional final garment. Stiffening the fabric sheets in this manner allows mature robotic technologies from other industries to be used in the garment industry, but requires the development of new manufacturing processes and tools to work with the novel textile-polymer sheets.

N. Castrillon, A. Rock: These authors contributed equally to this work.

✉ Tarek I. Zohdi
zohdi@me.berkeley.edu

[1] Department of Mechanical Engineering, University of California, Berkeley, Berkeley, United States

Published online: 09 August 2022

To introduce permanent bends easily and repeatedly along straight lines, this work will consider a process that uses heat to soften the thermoplastic binder, then applies mechanical force to bend the sheet along the softened line. Once the bend cools, the sheet solidifies and can be manipulated as a rigid body for additional assembly steps. One potential workflow using this idea involves supplying small robotic arms with a constantly heated metal attachment. To remain comparable to a human worker, the robotic arms must be general-purpose units capable of picking up, sewing, and bending a variety of work pieces.

The design of the bending tool was inspired by a "blade" tool used in robotic origami folding by researchers at Carnegie Mellon University [6] with the addition of a heating element. If this blade tool is hotter than the working temperature of the stiffening agent, it will greatly reduce the effort required to create permanent bends.

1.3 Variability and uncertainty in manufacturing

The study of UQ can be traced back to Sir Ronald Fisher's seminal paper, The Design of Experiments [7] published in 1935, where he discussed the principles of experimental design for the agricultural industry. Since then the study of variability and uncertainty has been widely used in wide-ranging applications such as the Antarctic ice sheet melting model [8], computational mechanics models [9], human toxicity dose estimation models [10], among others. Sacks et. al [11] provide a window into the state of the art of UQ in the late 1980s and Abdar et. al [12] gives a more contemporary review of the role of UQ in deep learning applications for optimization and decision making.

Several UQ frameworks have been constructed for performance evaluation of a wide array of manufacturing processes. These frameworks have shown merit in that they showcase how different sources of uncertainty in complex models can interact with each other, even in the total or partial absence of experimental data. Typically, Bayesian approaches estimate the network of uncertainty sources through a manufacturing system and then Monte Carlo approaches serve to calibrate the system for maximizing the accuracy of the UQ framework. In subtractive manufacturing, UQ has been performed for fatigue life predictions of welded structures [13] by studying variations in weld shape, residual stress, loading conditions and microstructure, as well as data uncertainty from measurement and numerical errors. UQ has also been used in milling stability region estimation in the parameter space [14] and in a deep drawing process [15] based on variations of material properties and friction forces inherent in the drawing operation. More recently, UQ frameworks have provided excellent approaches for studying highly complex methods such as selective electron beam melting (SEBM) [16]. Additionally, Hu and Mahadevan [17] provide a survey of current work in UQ for additive manufacturing and immediate needs. Lastly, Nannapaneni and Mahadevan [18] provide a systematic framework that propagate epistemic or aleatoric source of uncertainty in any manufacturing process application, showcasing examples in an injection molding process and a welding operation.

This work develops a thermal finite element model of the proposed garment assembly tool. This model is then used to assess the sensitivity of tool designs to environmental conditions such as the ambient temperature, and design specifications such as the blade dimensions or the input power. In Sect. 2, we provide more information about the construction of the blade tool, the formulation of a governing equation to solve for the thermal field, and the theory and uses of uncertainty quantification. Then, in Sect. 3 we apply the governing equation to a Finite Element Method (FEM) solver and how we use the thermal field solution to analyze the blade design for calculating sensitivities, characterizing the design space, and propagating uncertainties through the solver. We then show blade designs and a series of UQ examples in Sect. 4 before we provide our concluding remarks.

2 Background

2.1 Tool design

The tool considered in this work is inspired by an origami folding robot developed by Balkcom et al. [6] composed of an arm equipped with a long blade and a table top with a long opening. A sheet of paper is placed over the table opening and the robot arm guides the blade downwards, wiping the sheet of paper into the long opening. Then, a clamp mounted on the under side of the table closes the table opening, thus fixing the fold on the sheet of paper. Finally, the clamp retracts and the folded paper releases.

This work will focus exclusively on a part similar to the blade of the origami folding device, which directly contacts the sheet of paper. A simple framework for designs of our blade is shown in Fig. 1 and can be described by six dimensions: the thickness of the sheet metal used (not shown in figure), three lengths and two heights, each denoted L_1, L_2, L_3 and H_1, H_2 respectively. This geometry allows enough flexibility for a wide range of designs and minimizing the number design parameters. Future work could broaden the scope of possible designs by using a more complex geometry.

2.2 Governing equations

This work requires determining the thermal field resulting from a given heat source, surface losses, and internal conduction. Analysis is simplified using following assumptions:

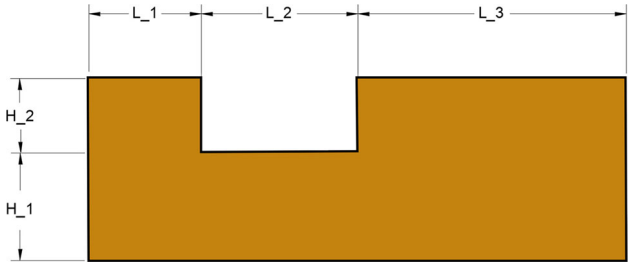

Fig. 1 Generic tool profile

- The thermal properties of the tool are not temperature-dependent in the regime of interest.
- Thermal expansion and other deformations are negligible.
- Thermal radiation may be approximated as black body radiation.
- The environment can be treated as an infinite heat sink, e.g., the ambient temperature is not coupled to the tool.
- Interactions between surfaces can be neglected, e.g., radiation from one area of the domain is not absorbed at another.

The governing equation for this thermal problem is a formulation of the first law of thermodynamics, written as:

$$\underbrace{\rho c \dot{T}}_{\text{thermal power}} = \underbrace{\nabla \cdot (k \nabla T)}_{\text{conduction}} + \underbrace{q}_{\text{source}} - \underbrace{l}_{\text{losses}} \tag{1}$$

The flux terms q and l require surface integrals, approximated for a given element e using Gaussian integration as:

$$\boldsymbol{S}^e = \int_{\delta\Omega e} \boldsymbol{\phi}^T \boldsymbol{\phi} dA = \sum_{p=1}^{g} \sum_{q=1}^{g} \boldsymbol{\phi}^T \boldsymbol{\phi} J w_p w_q \tag{2}$$

This model assumes that both convection and radiation contribute to the balance of energy. The thermal loss $\boldsymbol{l}$ is thus given by:

$$\boldsymbol{l} = \boldsymbol{c} + \boldsymbol{r} \tag{3}$$

Here, the vectors $\boldsymbol{c}$ and $\boldsymbol{r}$ represent surface area integrals of the domain.

$$\boldsymbol{c} = \underbrace{h\boldsymbol{S}}_{\boldsymbol{C}}(\boldsymbol{T} - \boldsymbol{T}_a), \qquad \boldsymbol{r} = \underbrace{\sigma \boldsymbol{S}}_{\boldsymbol{R}}(\boldsymbol{T}^4 - \boldsymbol{T}_a^4) \tag{4}$$

Where σ is the Boltzmann constant and h is the convective loss coefficient. The shorthand $\boldsymbol{C}$ and $\boldsymbol{R}$ is used for these surface integral matrices for convection and radiation losses, respectively, in further derivations.

The convective loss term enforces a Robin boundary condition [19] since it creates a linear relationship between the value and the gradient of the thermal field at some boundary locations. The radiation term is similar but enforces a nonlinear relationship.

2.3 Uncertainty quantification

The practice of uncertainty quantification (UQ) attempts to measure the sources of variation that affect the output of experimental systems and computational models. In manufacturing, UQ is used to study the contributions of aleatoric uncertainties such as the seemingly random effects from external, environmental effects or the local variations in the microstructure of the material that is being processed. These sources of variation can be modeled via Monte Carlo (MC) [20] or polynomial chaos methods [21], the former typically acting as the benchmark to the latter. Uncertainty can also be epistemic, dealing with errors due to the lack of knowledge or measurements.

UQ methods are normally used to solve forward uncertainty propagation problems. In these scenarios, previously-measured or estimated distributions of the inputs are propagated through a numerical solver to estimate the expected variations of the output. This topic has been studied extensively, for example in the application of structural mechanics [22]. An MC simulation is a simple and effective method for propagating the uncertainties since a set of input test points can be generated by randomly sampling each input variable's distribution. With enough input points, the variation of the output becomes evident and it can be quantified.

Another powerful use of UQ is to compute the sensitivity of the output with respect to each input individually. Perturbing any input within a small range, via a central difference scheme, for example, is a common strategy to locally approximate the derivative. However, the true sensitivity is defined in the limit as the perturbation range is reduced to zero, but it can also be computed analytically, if attainable, through direct differentiation of the governing equation. A high sensitivity to the perturbed input will yield relatively large changes to the output, and, inversely, a low sensitivity describes a relatively small to no change of the output value. Understanding these sensitivities can aid in design optimization [23–25].

Throughout this paper, the terms *sensitivity* and *derivatives* are used interchangeably.

When performing UQ for fitness of the design, an important output parameter, commonly referred as a quantity of interest (QoI), must be identified. In a typical application, a numerical simulation is used to produce a measure of a field, from which a chosen QoI can be calculated through post-processing. The QoI serves as a proxy for the effectiveness of a combination of input parameter values. Typical QoIs in structural simulations include maximum stress [26] and structural compliance [27], both calculated form the mechanical field of a deforming body.

This work presents a set of utilities for performing UQ for the design of the robotic bending attachment shown in Fig. 1. Our approach applies MC sampling and propagates uncertainties through a thermal FEM solver, computes the sensitivity of the QoI, and defines a hypersurface for design space characterization. The QoI selected in this study summarizes the temperature profile at the blade tool working edge, identified in Fig. 2 to aid us in predicting an acceptable or unacceptable fold procedure on the garment.

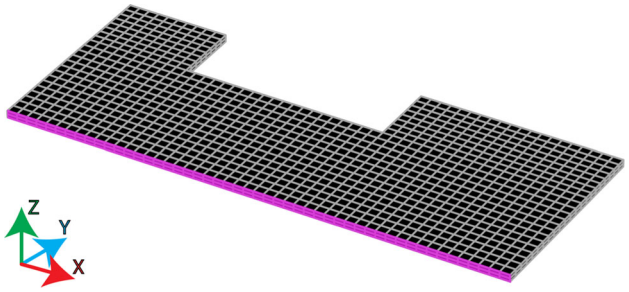

Fig. 2 Thermal field along the working edge, highlighted, is the key QoI for the bending process

3 Methods

3.1 Thermal FEM solver

Using a standard FEM formulation with thermal stiffness matrix $\boldsymbol{K}$ and mass matrix $\boldsymbol{M}$, Eq. 1 may be written as:

$$\dot{\boldsymbol{T}} = \boldsymbol{M}^{-1}\left(\boldsymbol{K}\boldsymbol{T} - \boldsymbol{C}(\boldsymbol{T} - \boldsymbol{T}_a) - \boldsymbol{R}(\boldsymbol{T}^4 - \boldsymbol{T}_a^4) + \boldsymbol{q}\right) \tag{5}$$

where $\boldsymbol{T}$ is a vector of temperature values for all nodes and $\boldsymbol{T}_a$ stores the ambient temperature. Using Forward Euler time integration, the discretized matrix-vector equation used to update the nodal temperatures:

$$\boldsymbol{T}^{n+1} = \boldsymbol{T}^n + \Delta t\ \dot{\boldsymbol{T}}. \tag{6}$$

3.2 Steady state solver

While transient temperature profiles, the response to perturbations, and properties such as the time required to reach operating temperatures all require time integration, the most important aspects of a tool's performance can be directly extracted from the temperature field at steady state. To resolve steady state thermal profiles, an efficient approximation method is necessary.

The steady state temperature may be defined by setting $\dot{\boldsymbol{T}} = 0$ in Eq. 5. This system is nonlinear and lends itself to an iterative solution scheme. To solve this system, Newton's method may be used to successively solve linearized approximations of the true system until a satisfactory numerical tolerance is achieved.

The inverse mass matrix $\boldsymbol{M}^{-1}$ from Eq. 6 may be factored out of non-trivial solutions:

$$\dot{\boldsymbol{T}} = 0 \rightarrow \boldsymbol{K}\boldsymbol{T} - \boldsymbol{C}(\boldsymbol{T} - \boldsymbol{T}_a) - \boldsymbol{R}(\boldsymbol{T}^4 - \boldsymbol{T}_a^4) + \boldsymbol{q} = 0 \tag{7}$$

where $\boldsymbol{T}_a$ is the ambient temperature.

Update terms are determined to refine the solution:

$$\boldsymbol{T}_{i+1} = \boldsymbol{T}_i + \boldsymbol{\Delta T}_i. \tag{8}$$

Here, i represents the number of iterations. Substituting this update rule into Eq. 7 yields:

$$\begin{aligned}&\boldsymbol{K}(\boldsymbol{T}_i + \Delta\boldsymbol{T}_i) - \boldsymbol{C}(\boldsymbol{T}_i + \Delta\boldsymbol{T}_i - \boldsymbol{T}_a)\\ &-\boldsymbol{R}\left((\boldsymbol{T}_i + \Delta\boldsymbol{T}_i)^4 - \boldsymbol{T}_a^4\right) + \boldsymbol{q} = 0\end{aligned} \tag{9}$$

A first-order Taylor expansion of the system about $\boldsymbol{T}_i$ with offset size $\Delta\boldsymbol{T}_i$ may be used to linearize the system:

$$(\boldsymbol{T}_i + \Delta\boldsymbol{T}_i)^4 \approx \boldsymbol{T}_i^4 + (4\boldsymbol{T}_i^3)\Delta\boldsymbol{T}_i \tag{10}$$

Substituting the approximation from Eq. 10 into Eq. 9 and rearranging yields:

$$\begin{aligned}&\underbrace{\left(\boldsymbol{C} - \boldsymbol{K} + 4\boldsymbol{R}\boldsymbol{T}_i^3\right)}_{\boldsymbol{A}}\underbrace{\Delta\boldsymbol{T}_i}_{\boldsymbol{x}}\\ &= \underbrace{(\boldsymbol{K} - \boldsymbol{C})\,\boldsymbol{T}_i - \boldsymbol{R}\boldsymbol{T}_i^4 + \left(\boldsymbol{R}\boldsymbol{T}_a^4 + \boldsymbol{q} + \boldsymbol{C}\boldsymbol{T}_a\right)}_{\boldsymbol{b}}\end{aligned} \tag{11}$$

Using this formulation, the steady state temperature may be iteratively determined to arbitrary precision.

For the remaining statistical analysis, the thermal solver may be treated as a black box that generates the nodal temperature array $\boldsymbol{T}(t)$ over time. Illustrative results are shown in Fig. 5.

3.3 Thermal field uncertainty quantification

In addition to directly improving key performance metrics, it is also desirable to ensure that the performance of the blade tool is predictable and agnostic to environmental disturbances or imprecise tool construction. First, sensitivity data can inform the tool designers about design options that yield increasingly robust designs. Resiliency of the output thermal field to perturbations of a certain input parameter translates to a viable blade design. Second, parameter studies give insight about the design space and the output's expectation.

3.3.1 The quantity of interest

The design of a thermal blade tool requires defining its geometry, as well as construction material and a heat source, in hopes of contributing to a desired performance. The metric for the desired performance is what is called a quantity of interest (QoI). Typically, QoI data is a single scalar value for a given design point, and the output of a post-processing step on the field solution from the numerical solution.

The primary QoI selected for this study is the temperature range along the working edge of the blade at steady state. This region of interest is shown in Fig. 2.

Minimizing this QoI is a proxy for a consistent folding operation on the garment work piece. A wide temperature range at this edge will create uneven softening and result in unpredictable bending characteristics. Accordingly, successful tool designs will minimize temperature ranges in this area.

There are a myriad of QoI metrics that we can analyze with our UQ utility. An example would be the time the blade requires to reach operating temperatures. We estimate that a blade with rough outer dimensions of $0.2 \times 0.35m$ can take up to 20 minutes to reach its steady state temperature. Long wait times will reduce productivity on the manufacturing floor, driving the need for designs that minimize this particular QoI.

3.3.2 Data generation

The structure of the output UQ data is a 2-dimensional array with labeled columns and rows, sized $m \times (n+1)$, where m is the number of queried design points and n is the number of input parameters and the extra column stores QoI data. We can then analyze the design of the blade tool in three ways: sensitivity computations, design space characterization, and the propagation of uncertainty through the solver.

The aim of sensitivity computations is to approximate the local gradient of the QoI with respect to the design parameters. A typical method is using central differences. This type of analysis runs on a single query point, returning its QoI value and its partial derivatives. Explicitly, the user-specified query point $P(v_1, v_2, \ldots, v_n)$ is perturbed independently on each variable via a user-specified resolution, δ. The perturbation of design variable v_j is computed by:

$$P_{v_j+} = P\left(v_1, v_2, \ldots, (1+\delta)v_j, \ldots, v_n\right)$$
$$P_{v_j-} = P\left(v_1, v_2, \ldots, (1-\delta)v_j, \ldots, v_n\right).$$

The QoI value is calculated by $\mathcal{Q}^+ = f\left(P_{v_j+}\right)$ and $\mathcal{Q}^- = f\left(P_{v_j-}\right)$, where function f represents the thermal FEM solver. The sensitivity due to v_j is:

$$S_j = \frac{\partial \mathcal{Q}}{\partial v_j} \approx \frac{\mathcal{Q}^+ - \mathcal{Q}^-}{P_{v_j+} - P_{v_j-}}. \tag{12}$$

The MC simulation can also be leveraged to explore the design space, either across the entire space within its boundaries or in a particular region of interest. The design space may be defined with an orthogonal basis, where each dimension corresponds to a design parameter. In this study, a predetermined number of query points are generated from a translational propagation Latin hypercube (TPLH) sampling design algorithm by [28]. This algorithm ensures a fast, high-quality sampling design that is modular depending on the chosen number of query points. Table 1 showcases a sample symbolic design with 4 design points, and thus 4 levels are queried per variable (low, mid-low, mid-high, and high). In the spirit of Latin hypercube sampling, note that each level is represented once for each input variable.

Lastly, we can propagate the distributions of the inputs through the solver to discover a resulting output distribution of the QoI. Typically, the distributions of the inputs have been previously measured experimentally or they may be estimates. The design points can then be randomly sampled from these input distributions until a pre-determined number of samples has been reached, or until the QoI distribution does not change, outside a tolerance, with subsequent samples.

Aided by the definition of sensitivity analysis by [29], we can see that this type of analysis attempts to explain the individual contributions of each design parameter to the output distribution. In other words, the major contributors to the uncertainty of the QoI can be identified, know as factor prioritization, and the least influential parameters can be removed from the set of design inputs, know as factor fixing.

As a best practice, experimental data should calibrate estimates of the input distributions, e.g. with Bayesian inference methods. However, this is beyond the scope of this study. Our computational thermal tool for garment fabrication is agnostic to the distributions of the inputs and so it is the user's task to identify the most accurate data to employ.

4 Results

In this section, numerical thermal field results are shown for a characteristic thin, rectilinear tool with a slot geometry subjected to varied thermal loads. The resulting thermal field data will be queried for the range of steady state temperatures at the working edge (the QoI). We will showcase the usefulness of this data: calculate local sensitivities, map out the design space, and quantify the uncertainty of the QoI via MC propagation.

Table 1 Example of a sampling design from the translational propagation Latin hypercube algorithm by [28] with 4 data points. Therefore, each input variable is discretized into 4 levels: low, mid-low, mid-high, and high

	Convection Coeff.	Reflectivity	Base Height	Left Pad Width
Design point 1	low	med-low	med-high	low
Design point 2	med-high	med-high	high	med-low
Design point 3	high	low	low	med-high
Design point 4	med-low	high	med-low	high

The meshing and simulation tool is able to simulate and visualize the performance of varied blade designs. For moderate resolutions like those shown below, the entire meshing, numerical solution with Eq. 11, and plotting procedure takes up to 4 seconds per design on a modern laptop.

4.1 Numerical example

The thermal simulation model takes selected geometric and thermal design parameters and solves for the resulting thermal field at steady state and over time starting with given initial conditions.

Example results with two different heat sources and construction materials are shown in Figs. 3 and 4 to demonstrate the inputs for quantifying the uncertainty of the thermal field. Four possible designs are considered, using either aluminum or copper as a construction material and either a thin heated wire through the middle of the tool or a pair of rectangular thermoelectric pads on the sides. In all designs, 200 Watts of thermal power is applied as a flux boundary condition uniformly over the defined source geometry.

The thermal properties of aluminum and copper are assumed to be constant with respect to temperature and are given by Table 2.

The following dimensions were used for all example designs:

- $L_1 = 7.5\ cm$
- $L_2 = 15\ cm$
- $L_3 = 15\ cm$
- $H_1 = 10\ cm$
- $H_2 = 5\ cm$
- $thickness = 5\ mm$

Two different heat source geometries will be considered: rectangular pads on the front side of the blade or a narrow strip wrapped all the way around the blade to imitate a coil of wire, referred to as the pad design and wire design. These source regions will be idealized as constant within rectangular regions orthogonal to the $\hat{z}$ direction, described by upper and lower bounds in the $\hat{x}$ and $\hat{y}$ directions and an exact coordinate $\hat{z}$.

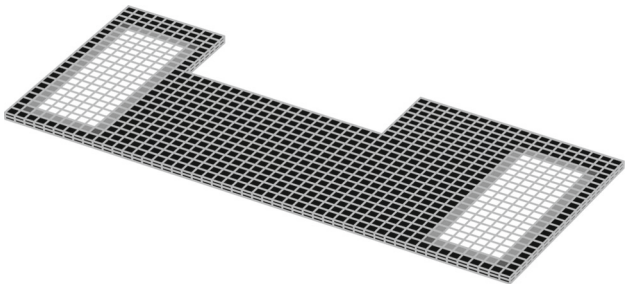

Fig. 3 Schematic of example "pad" heat source

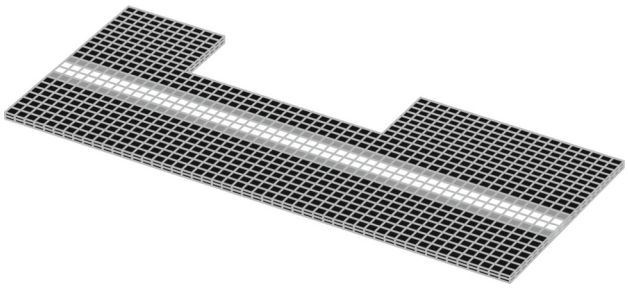

Fig. 4 Schematic of example "wire" heat source

Table 2 Thermal properties

Property	Aluminum	Copper
$c\ [J/(kg \cdot K)]$	920	375
$\rho\ [kg/m^3]$	2720	8960
$k\ [W/(m \cdot K)]$	237	400

For a specified power p_i, a source term q_i is modeled with the following form:

$$q_i(x, y, z) = \begin{cases} & (x_{max,i} \geq x \geq x_{min,i})\ \& \\ \frac{p_i}{\alpha_i} & (y_{max,i} \geq y \geq y_{min,i})\ \& \\ & (z = z_i) \\ 0 & \text{otherwise} \end{cases} \tag{13}$$

Where α_i is the area of a given source region:

$$\alpha_i = (x_{max,i} - x_{min,i}) \times (y_{max,i} - y_{min,i}).$$

Note that numerical integration of step functions using Gaussian quadrature is not exact since it is not possible to exactly

Table 3 Dimensions for numerical examples in centimeters

i	$x_{min,i}$	$x_{max,i}$	$y_{min,i}$	$y_{max,i}$	z_i
1	1.875	5.625	2.500	12.500	0.500
2	31.875	35.625	2.500	12.500	0.500
3	0.000	37.500	6.167	7.167	0.000
4	0.000	37.500	6.167	7.167	0.500

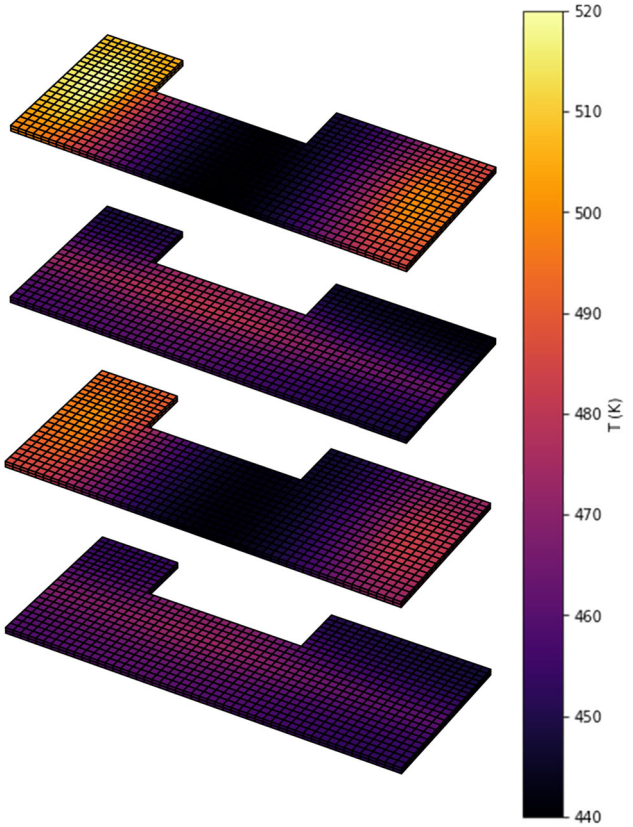

Fig. 5 Example steady state thermal fields. Top to bottom: copper with pads, copper with wire, aluminum with pads, aluminum with wire

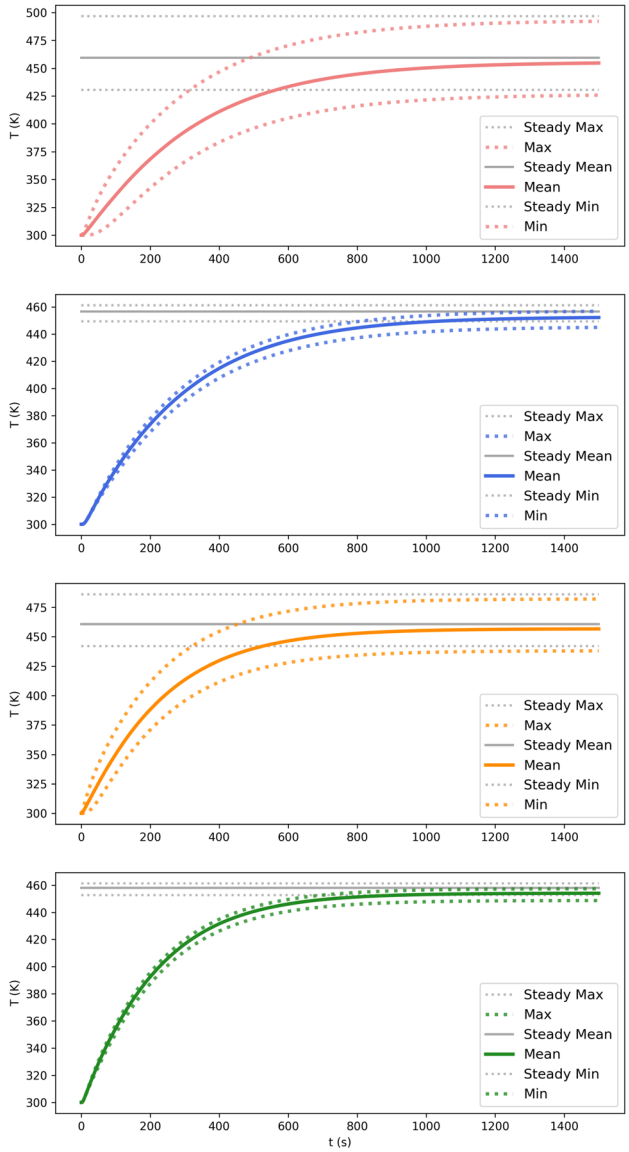

Fig. 6 Example transient and steady thermal fields along working edge. Top to bottom: copper with pads, copper with wire, aluminum with pads, aluminum with wire

fit a general step function with a polynomial. Any piece-wise source term, regardless of form, may result in integration errors. The impact of discontinuities may be reduced by refining the mesh.

Both the pad and wire designs will have two source regions, defined by

$$q_{pad} = q_1 + q_2 \quad \text{and} \tag{14}$$

$$q_{wire} = q_3 + q_4. \tag{15}$$

The pad geometries are defined by the values shown in table 3.

All example source regions impart 100 W of thermal power for a total of 200 W of thermal power per design. The source regions with these parameters are shown in Figs. 3 and 4. Note that the second source region for the wire design is on the bottom side of the blade, directly below the visible region. Elements colored white are entirely within the source region, elements colored black are entirely outside, and elements colored gray are on the border.

It can be seen both qualitatively in Fig. 5 and quantitatively in Fig. 6 that the rectangular sources concentrate heat and create a significant deviation in temperature. The wire sources keep a much lower peak temperature since the source region has a much larger perimeter for heat to dissipate outward through. Additionally, since the wire source region is closer to the working edge on average, it produces a more uniform

profile as reflected in the greatly reduced gap between the minimum and maximum edge temperatures shown in Fig. 6.

The thermal profiles at steady state with copper or aluminum construction are very similar with the exception of higher edge temperatures with copper when combined with pad heat sources since the higher conductivity of copper spreads the hot spot under the source toward the edge more effectively. Since neither material is clearly superior for the quantities of interest in this study, considerations like weight and cost should drive the selection of materials, not the thermal profile along the front edge.

While inspection and comparison of possible designs is one possible use of the thermal model of the bending tool, using sensitivity analysis to compare designs automatically can offer greater insight into the effectiveness of different design choices.

4.2 Quantifying the uncertainty

Now, here we present sample UQ data structures and results for the utilities introduced in Sect. 3.3: sensitivity calculations for a query point, characterizations of design space, and propagation of the input uncertainties. For all results that follow, the temperature range QoI is calculated as:

$$\mathcal{Q} = max\ \tilde{T} - min\ \tilde{T}, \tag{16}$$

where $\tilde{T} \in \{T(x, y, z) \mid y = 0\}$ for a blade tool oriented as in Fig. 2.

The results that follow pertain to a copper tool heated via two thermal pads mounted on the areas outlined by the white grid cells in Fig. 3.

4.2.1 Sensitivity calculations

Here, we compute the gradient of $\mathcal{Q}$ with respect to each design parameter as shown in Eq. 12. Table 4 demonstrates the data structure of the output array: the query point, the temperature range value, and the sensitivity values. This data pertains to a relatively large perturbation, $\delta = 10^{-4}$, but the sensitivities can be computed with any positive resolution.

At the chosen resolution, sensitivity results suggest that all design variables have an inverse relation to the temperature range at the working edge. These results confirm our intuition. The environmental parameters will tend to quell hot and cold spots, thus reducing local temperature spikes. Low values of the geometric parameters enlarge the size of the slot and this tends to constrain and guide the flow of heat towards a particular region of the working edge, thus producing warmer spots.

Finding actual deviations of the QoI $\Delta\mathcal{Q}$ from a given design parameter perturbation, e.g. perturbations of the material thermal reflectivity, can be accomplished by

$$\Delta\mathcal{Q} = \frac{\partial\mathcal{Q}}{\partial\epsilon}\Delta\epsilon, \tag{17}$$

where $\Delta\epsilon = \epsilon - (1-\delta)\epsilon = \delta\epsilon$ is the perturbation amount. This computation also normalizes all sensitivities to the units of the QoI for directly comparing the sensitivity of $\mathcal{Q}$ due to each design variable.

These sensitivity results are the cornerstone for gradient-based optimization routines such as the gradient descent or the conjugate gradient methods.

4.2.2 Characterizing the design space

This utility outputs data for building a response hypersurface of the design space, with its local value $\mathcal{Q}_i$ at each design point $P_i(h, \epsilon, H_1, L_1)$. From a predetermined axis-aligned, 4-dimensional bounding cube and a chosen number of design points, we sample the space using the fast, optimal TPLH design. The data in Table 5 are results of a 4-point sampling in our 4-dimensional design space following the design example in Table 1. The design parameters spanned the following bounds:

- $h = [0.0, 100.0]\frac{W}{m^2 \cdot K}$
- $\epsilon = [0.1, 1.0]$
- $H_1 = [0.050, 0.150]m$
- $L_1 = [0.050, 0.160]m$

Of course, to effectively capture a useful hypersurface in a 4-dimensional space, the TPLH sampling design must incorporate a considerably higher quantity of design points than shown in Table 5.

4.2.3 Propagating the uncertainties of the inputs

We now assume that we can estimate each design parameter distribution based on typical laboratory settings. Our UQ utility is capable of sampling any distribution in standard Python packages in addition to any user-built density function, making it versatile for using corrected design parameter distributions.

Here, we model the case where the blade tool is made of copper and there is an environmental control in the laboratory. Hence, the convection coefficient and the material reflectivity are only subject to random variations, best modelled by a normal distribution with a standard deviation smaller than 10% of the mean. In the case of the geometrical parameters, we can say that the user is interested in exploring all possible dimensions with equal interest and so H_1 and L_1 are assigned uniform distributions, bounded by physical restrictions imposed by the thermal pad size. In summary:

Table 4 Sample output from the design sensitivity utility via central differences and $\delta = 10^{-4}$. Included is the query design point, the temperature range at the working edge (QoI) for the query design point, and the sensitivity of the QoI

Query Point				Temp. Range	Temperature Range Sensitivity			
h	ϵ	H_1	L_1	$\mathcal{Q}$	$\frac{\partial \mathcal{Q}}{\partial h}$	$\frac{\partial \mathcal{Q}}{\partial \epsilon}$	$\frac{\partial \mathcal{Q}}{\partial H_1}$	$\frac{\partial \mathcal{Q}}{\partial L_1}$
$[W/(m^2 \cdot K)]$		$[m]$	$[m]$	$[K]$	$[K/(\frac{W}{m^2 \cdot K})]$	$[K]$	$[K/m]$	$[K/m]$
40	0.7	0.1	0.11	15.59	−0.086	−1.030	−141.0	45.2

Table 5 Sample output from the design space characterization utility. The design space is 4-dimensional and 4 design points were output from a TPLH sampling design. Included in the data is are the design points and the temperature range at the working edge (QoI)

	Design Parameters				Temp. Range
	h $[W/(m^2 \cdot K)]$	ϵ	H_1 $[m]$	L_1 $[m]$	$\mathcal{Q}$ $[K]$
Design point 1	0.0	0.4	0.117	0.050	22.23
Design point 2	66.7	0.7	0.150	0.087	6.52
Design point 3	100.0	0.1	0.050	0.123	34.17
Design point 4	33.3	1.0	0.083	0.160	7.92

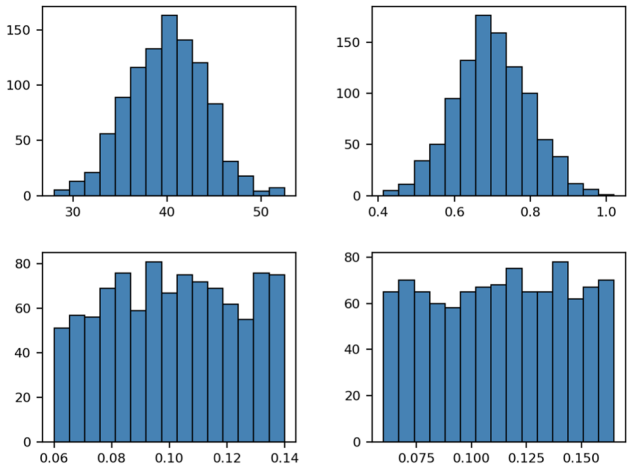

Fig. 7 Input distributions of the design parameters. A normal distribution is assumed for the environmental variables and a uniform distribution is assumed for the geometrical variables. Clockwise from top left: h, ϵ, left pad width, right pad width

- $h \sim \mathcal{N}(40, 4.0^2)$
- $\epsilon \sim \mathcal{N}(0.7, 0.1^2)$
- $H_1 \sim \mathcal{U}(0.06, 0.14)$
- $L_1 \sim \mathcal{U}(0.06, 0.165)$

The output data structure is identical to Table 5. We have decided to sample 1, 000 points, each taking in average of 3.67 s to generate a QoI value on a 2.3 GHz quad-core Intel Core i7 processor. Fig. 7 has frequency plots for the input parameter values that were sampled.

The MC simulation propagated the input distributions through the thermal FEM solver. The output distribution for the temperature range at the working edge QoI is shown as a frequency plot and a kernel density estimation plot, Figs. 8

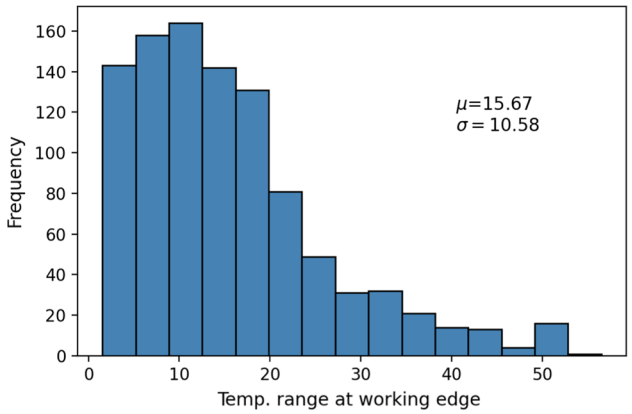

Fig. 8 Output distribution of the temperature range at the working edge, histogram

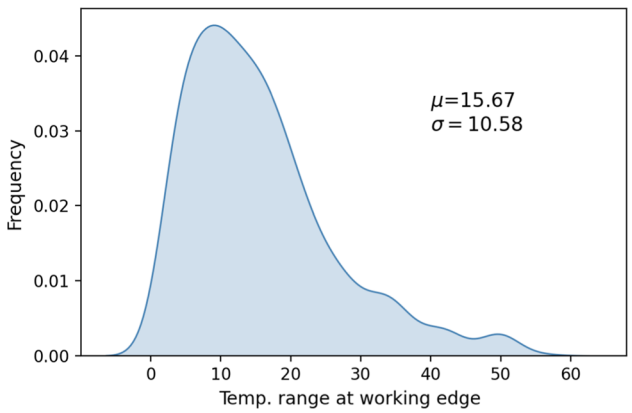

Fig. 9 Output distribution of the temperature range at the working edge, probability density

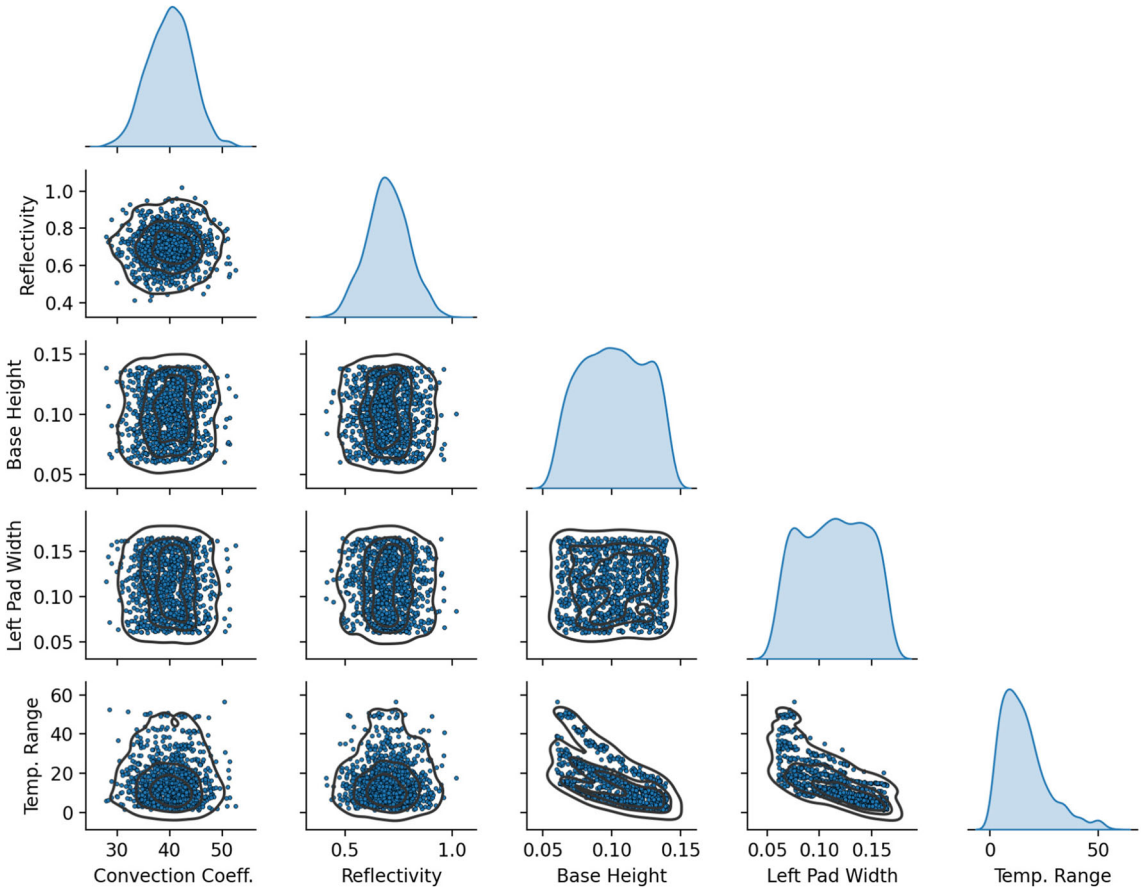

Fig. 10 Pairwise plots for the design parameters and the temperature range at the working edge. The diagonals showcase the continuous probability density curve for each. The off-diagonals show relationships between each pair. The bottom row shows the contributions of each design parameter to the distribution of the QoI

and 9 , respectively. Note that the QoI distribution has grossly deviated from the input distributions: it neither exhibits a uniform nor a normal distribution. Also, since the output distribution is purely empirical, every set of data from different batches of 1,000 sample points results in a slightly different QoI distribution, but the shape will always exhibit a positive third moment (skewness) measure.

Pairwise plots as the ones in Fig. 10 provide further insight about the QoI uncertainty. The plots on the off diagonals show the 2-dimensional scatter, highlighting hidden relationships between all input-input or input-QoI pairs. We can see that on the bottom line of scatter plots, for all input variables, the greatest density of points is manifested towards the lower bound of the temperature range QoI. In other words, closer to the $\mathcal{Q} = 0$ K versus the 60 K vicinity. This pattern in the scatter plots is the major contributor to a positive skewness of the output distribution.

Furthermore, we can also observe from these scatter plots that varying the environmental variables do not contribute to large changes in the temperature range QoI. However, the dimensions of the blade do contribute inversely to changes in the expected value of the QoI. For instance, a base height H_1 dimension closer to the higher bound will contribute to a lower expected temperature range QoI value than a shorter base dimension.

Propagating the input uncertainties through the solver is a powerful utility to set the expectations for the performance of the system, in this case the blade tool temperatures. Let's say that for a particular folding procedure application a temperature range at the working edge of more than 30 K is unacceptable. Therefore, the blade tool designers must make a decision whether the output distribution represented in Figs. 8 and 9 represents a risk of undesirable performance of the tool.

5 Conclusion

This work presents a design sensitivity analysis of a heated blade tool for robotic folding of thermoplastic-stiffened cloth for garment production. A numerical example showing how this model can inform design decisions, and particularly distinguish between strongly and weakly important design

decisions, shows how a designer could use this model to inform design iteration and improve key quantities of interest for high performance on a production line.

Funding This work was partially funded by the Siemens Corporation and the Advanced Robotics Manufacturing (ARM) Institute. Professor Zohdi's work is supported by AFRI Competitive Grant no. 2020-67021-32855/project accession no. 1024262 from the USDA National Institute of Food and Agriculture. This grant is being administered through AIFS: the AI Institute for Next Generation Food Systems. https://aifs.ucdavis.edu.

Data Availability The data used in this work was generated by code written by the authors. It may be obtained from the contributing authors upon reasonable request.

Code Availability The code used in this work may be obtained from the contributing authors upon reasonable request.

Declarations

Conflict of interest The authors declare no competing interests.

References

1. Nayak R, Padhye R (2018) Introduction to Automation in Garment Manufacturing. In: Automation in garment manufacturing. Elsevier, pp 1–27
2. Li X, Hui EC, Lang W, Zheng S, Qin X (2020) Transition from factor-driven to innovation-driven urbanization in china: A study of manufacturing industry automation in dongguan city. China Econ Rev 59:101382
3. Schrage S, Huber K (2018) 15 living wages in international supply chains and the capability approach. New frontiers of the capability approach, 351
4. Maitin-Shepard J, Cusumano-Towner M, Lei J, Abbeel P (2010) Cloth grasp point detection based on multiple-view geometric cues with application to robotic towel folding. In 2010 IEEE International Conference on Robotics and Automation. IEEE, 2308–2315
5. Zornow J (2020) Sewbo, inc.,
6. Balkcom D (2004) Robotic origami folding. PhD thesis, Citeseer
7. Fisher R A (1935) The design of experiments. The design of experiments., 1st Ed,
8. Bulthuis K, Arnst M, Sun S, Pattyn F (2019) Uncertainty quantification of the multi-centennial response of the antarctic ice sheet to climate change. Cryosphere 13(4):1349–1380
9. Liang B, Mahadevan S (2011) Error and uncertainty quantification and sensitivity analysis in mechanics computational models. Int J Uncertain Quantif 1(2):147–161
10. Isukapalli SS, Roy A, Georgopoulos PG (1998) Stochastic response surface methods (srsms) for uncertainty propagation: application to environmental and biological systems. Risk Anal 18(3):351–363
11. Sacks J, Welch WJ, Mitchell TJ, Wynn HP (1989) Design and analysis of computer experiments. Stat Sci 4:409–423
12. Abdar M, Pourpanah F, Hussain S, Rezazadegan D, Liu L, Ghavamzadeh M, Fieguth P, Cao X, Khosravi A, Rajendra A U, et al. (2020) A review of uncertainty quantification in deep learning: Techniques, applications and challenges. arXiv preprint arXiv:2011.06225
13. Shiraiwa, T, Briffod, F, Enoki M (2017) Uncertainty quantification of fatigue life prediction in welded structures using microstructure-based simulations. In International Conference on New Trends in Fatigue and Fracture, pages 329–334. Springer
14. Li K, He S, Liu H, Mao X, Li B, Luo B (2020) Bayesian uncertainty quantification and propagation for prediction of milling stability lobe. Mech Syst Signal Process 138:106532
15. Huang C, Radi B, El Hami A (2016) Uncertainty analysis of deep drawing using surrogate model based probabilistic method. The International Journal of Advanced Manufacturing Technology 86(9):3229–3240
16. Wang Z, Liu P, Ji Y, Mahadevan S, Horstemeyer MF, Zhen H, Chen L, Chen L-Q (2019) Uncertainty quantification in metallic additive manufacturing through physics-informed data-driven modeling. JOM 71(8):2625–2634
17. Zhen H, Mahadevan S (2017) Uncertainty quantification and management in additive manufacturing: current status, needs, and opportunities. The International Journal of Advanced Manufacturing Technology 93(5):2855–2874
18. Nannapaneni S, Mahadevan S (2014) Uncertainty quantification in performance evaluation of manufacturing processes. In 2014 IEEE International Conference on Big Data (Big Data), pages 996–1005. IlEEE
19. Könnö J, Schötzau D, Stenberg R (2011) Mixed finite element methods for problems with robin boundary conditions. SIAM J Numer Anal 49(1):285–308
20. Lozanovski B, Downing D, Tran P, Shidid D, Qian M, Choong P, Brandt M, Leary M (2020) A monte carlo simulation-based approach to realistic modelling of additively manufactured lattice structures. Addit Manuf 32:101092
21. Tapia G, King W, Johnson L, Arroyave R, Karaman I, Elwany A (2018) Uncertainty propagation analysis of computational models in laser powder bed fusion additive manufacturing using polynomial chaos expansions. J Manuf Sci Eng 140(12):121006
22. Soize C (2012) Stochastic models of uncertainties in computational mechanics. American Society of Civil Engineers
23. Taber A, Castrillon N, Kumar G (2021) Sensitivity computation of integral quantities with moment derivatives [manuscript submitted for publication]. Journal of mechanical design
24. Allaire G, Jouve F, Toader A-M (2004) Structural optimization using sensitivity analysis and a level-set method. J Comput Phys 194(1):363–393
25. Tortorelli DA, Michaleris P (1994) Design sensitivity analysis: overview and review. Inverse problems in Engineering 1(1):71–105
26. Holmberg E, Torstenfelt B, Klarbring A (2013) Stress constrained topology optimization. Struct Multidiscip Optim 48(1):33–47
27. Jun W, Clausen A, Sigmund O (2017) Minimum compliance topology optimization of shell-infill composites for additive manufacturing. Comput Methods Appl Mech Eng 326:358–375
28. Viana FAC, Venter G, Balabanov V (2010) An algorithm for fast optimal latin hypercube design of experiments. Int J Numer Meth Eng 82(2):135–156
29. Saltelli A, Aleksankina K, Becker W, Fennell P, Ferretti F, Holst N, Li S, Qiongli W (2019) Why so many published sensitivity analyses are false: A systematic review of sensitivity analysis practices. Environmental modelling & software 114:29–39